Photoelectrochemical Properties of TiO_2 Nanowire Arrays: A Study of the Dependence on Length and Atomic Layer Deposition Coating

Yun Jeong Hwang,[†,§] Chris Hahn,[†,§] Bin Liu,[†] and Peidong Yang[†,‡,§,*]

[†]Department of Chemistry and [‡]Department of Materials Science and Engineering, University of California, Berkeley, California 94720, United States and [§]Materials Sciences Division, Lawrence Berkeley National Laboratory, Berkeley, California 94720, United States

ABSTRACT We report that the length and surface properties of TiO_2 nanowires can have a dramatic effect on their photoelectrochemical properties. To study the length dependence, rutile TiO_2 nanowires (0.28−1.8 μm) were grown on FTO substrates with different reaction times (50−180 min) using a hydrothermal method. Nanowires show an increase in photocurrent with length, and a maximum photocurrent of 0.73 mA/cm^2 was measured (1.5 V *vs* RHE) for 1.8 μm long nanowires under AM 1.5G simulated sunlight illumination. While the incident photon to current conversion efficiency (IPCE) increases linearly with photon absorptance ($1-10^{-\alpha\times\text{length}}$) with near band gap illumination ($\lambda = 410$ nm), it decreases severely at shorter wavelengths of light for longer nanowires due to poor electron mobility. Atomic layer deposition (ALD) was used to deposit an epitaxial rutile TiO_2 shell on nanowire electrodes which enhanced the photocatalytic activity by 1.5 times (1.5 V *vs* RHE) with 1.8 μm long nanowires, reaching a current density of 1.1 mA/cm^2 (61% of the maximum photocurrent for rutile TiO_2). Additionally, by fixing the epitaxial rutile shell thickness and studying photoelectrochemical (PEC) properties of different nanowire lengths (0.28−1.8 μm), we found that the enhancement of current increases with length. These results demonstrate that ALD coating improves the charge collection efficiency from TiO_2 nanowires due to the passivation of surface states and an increase in surface area. Therefore, we propose that epitaxial coating on materials is a viable approach to improving their energy conversion efficiency.

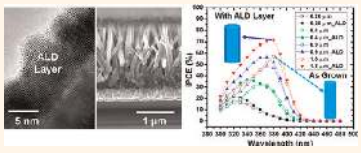

KEYWORDS: TiO_2 nanowire · atomic layer deposition · photoanode · photoelectrochemical water splitting · length dependence · charge collection efficiency

Artificial photosynthesis has been considered as a desirable approach to supply clean energy since it can capture and convert the energy of sunlight into the chemical bonds of a fuel such as hydrogen.[1] Solar water splitting to convert water into hydrogen and oxygen is one of the most attractive forms of artificial photosynthesis. Since Honda and Fujishima demonstrated water splitting with TiO_2 in 1972,[2] the photoanodic properties of TiO_2 (rutile) have been widely studied[3−7] because it is highly resistant to photocorrosion, nontoxic, abundant, and cheap. However, TiO_2 has too wide of a band gap (3.0 eV)[8] to absorb sunlight in the visible region, and its low electron mobility (1 cm^2 V^{-1} s^{-1})[9] and short minority carrier (hole) diffusion length (10−100 nm)[8,10] limit its quantum efficiency even in the UV region.

Nanostructured TiO_2 has been demonstrated[11−14] to increase its quantum efficiency for water splitting since recombination can be mitigated by decreasing the distance necessary for the minority carrier to diffuse to the surface. In particular, one-dimensional (1D) nanostructures such as nanowire and nanotube arrays are advantageous over planar geometries because they can decouple the directions of light absorption and charge carrier collection.[15−18] TiO_2 nanowire arrays can have efficient charge transfer at the TiO_2/electrolyte interface despite a short hole diffusion length because the hole only needs to diffuse across the radius of the nanowire.[1,15] However, the low electron mobility in rutile TiO_2 can be an obstacle because electrons must transport along the nanowires to reach the electrical contact.[19] To date, 1D nanostructured TiO_2 has been investigated, but the dependence of PEC activity on length has not been systematically studied.

The surface properties of nanostructures are especially important to the overall charge collection efficiency since they can influence the recombination velocity and the chemical reaction dynamics. Surface states in nanostructures can be different depending on the preparation method.[10] One method to decrease

* Address correspondence to p_yang@berkeley.edu.

Received for review February 15, 2012 and accepted May 15, 2012.

Published online May 23, 2012
10.1021/nn300679d

surface recombination velocity is a surface coating.[20] Atomic layer deposition (ALD) is a coating technique that can passivate surface states to decrease the surface recombination velocity.[21] Its layer-by-layer deposition allows for highly conformal coating even on the dense and rough surfaces of certain nanostructures. Formal *et al.* demonstrated that a thin layer of Al_2O_3 deposited by ALD on nanostructured Fe_2O_3 can lower the photocurrent onset potential by passivating surface states.[22]

For the ALD coating to have a beneficial effect on the water splitting efficiency, several factors should be considered for choosing the right material. First, the interface between the ALD layer and the semiconductor material should be considered. For example, a large lattice mismatch can cause non-uniform coating and additional defects due to strain. For materials with a large lattice mismatch, it is possible to introduce a buffer layer to relax the strain at the interface. Paracchino *et al.* used ZnO and Al_2O_3 buffer layers to relax the strain at the interface which can increase the stability of a TiO_2 ALD layer on a p-Cu_2O electrode.[23] Second, the ALD layer should have the right band alignments with the semiconductor to prevent additional energetic barriers for charge carriers.[23,24] The valence band potential of the ALD shell should be equal to or higher than that of rutile TiO_2 to allow efficient hole transfer. In addition, the valence band potential of the ALD shell should be lower in energy than the water oxidation potential to allow the reaction to be thermodynamically favorable. A coating of ALD TiO_2 on rutile nanowire arrays could satisfy all of the aforementioned factors.

Here, we use TiO_2 nanowires as a model system for photoelectrochemical (PEC) water splitting to conduct a quantitative study on the dependence of the IPCE on nanowire length and ALD TiO_2 coating. From these results, we demonstrate that the efficiency of the TiO_2 nanowire arrays can be improved by increasing the length of the nanowires as well as by coating the surface with an ALD shell. These geometric studies of TiO_2 nanowire arrays can offer a strategy toward optimizing the energy conversion efficiency with other semiconductor materials in solar water splitting.

RESULTS AND DISCUSSION

To study the photoanodic activity dependence on the length of TiO_2 nanowires, four different lengths of TiO_2 nanowire arrays were prepared on FTO from a hydrothermal method[25] by controlling the growth time between 50 and 150 min at the same growth temperature (200 °C). When the growth time exceeded 3 h, TiO_2 nanowire arrays started to delaminate from the FTO substrate and form a white thin film due to the competition between crystal growth and dissolution at the FTO–nanowire interface.[25] Figure 1 shows top-down scanning electron microscope (SEM) images

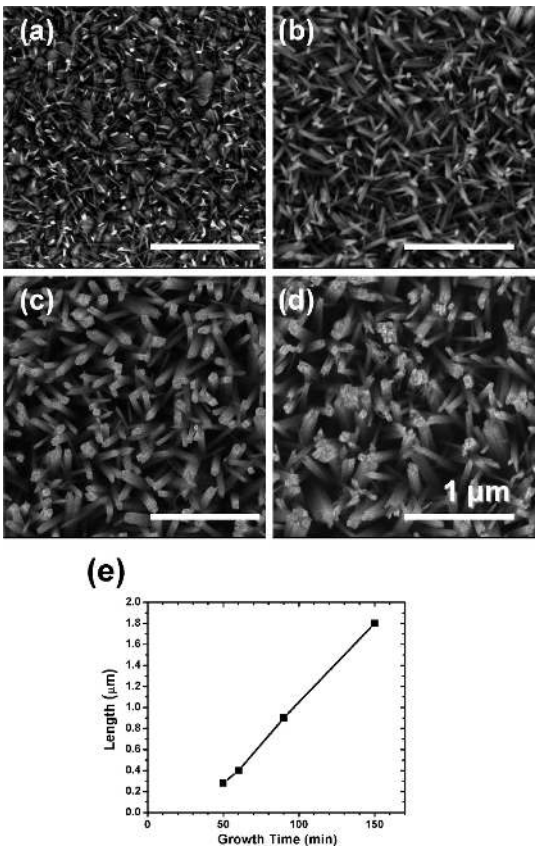

Figure 1. SEM images of hydrothermally grown TiO_2 nanowires on FTO substrates for (a) 50 min, (b) 60 min, (c) 80 min, and (d) 150 min at 200 °C. (e) Nanowire lengths were plotted *vs* time, showing that the growth rate is linear.

of TiO_2 nanowire arrays grown on FTO. The bare FTO substrate was still visible within 50 min (Figure 1a) due to the short length and low density coverage of nanowire arrays. After 60 min, TiO_2 nanowire arrays completely covered the FTO substrate (Figure 1b–d). The average lengths of the nanowire arrays were measured (see Figure 5) to be 0.28 (±0.03), 0.4 (±0.05), 0.9 (±0.08), and 1.8 (±0.1) μm for growth times of 50, 60, 80, and 150 min, respectively. The length of the nanowires linearly increased with time (T) (Figure 1e, eq 1) at a growth rate of 0.015 μm/min.

$$\text{length } (\mu\text{m}) = 0.015 \times (T \text{ (min)} - 33) \quad (1)$$

A delay of 33 min was seen in the nucleation of TiO_2 nanowires due to the time required to heat the autoclave up to 200 °C and supersaturation of TiO_2.

PEC measurements were performed on four different lengths of TiO_2 nanowire arrays (Figure 2) with the electrodes mentioned above. Photocurrent measurements (Figure 2a) show that the onset potentials of photocurrents (0.1 V *vs* RHE) remain the same as the length of the nanowires increases. The onset potential of photocurrents is mainly determined by the properties of rutile TiO_2, such as the over potential of the

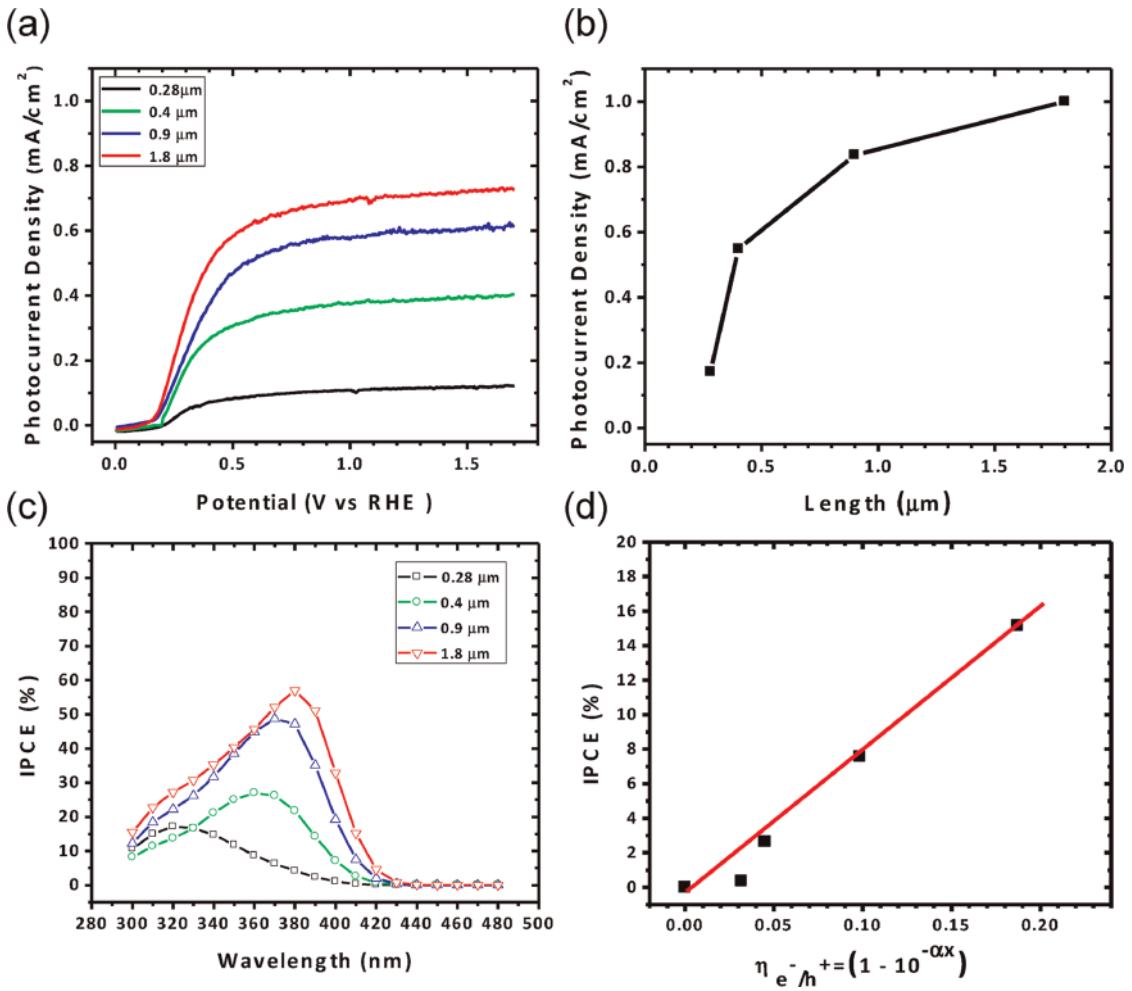

Figure 2. (a) Plots of photocurrent density *vs* RHE for TiO_2 nanowire arrays show an increase in photocurrent with nanowire length. (b) Photocurrent densities are compared at 1.5 V *vs* RHE for different nanowire lengths and show that the current begins to saturate with longer nanowires. (c) IPCE (1.5 V *vs* RHE) of TiO_2 nanowire array electrodes shows a shift in λ at the maximum EQE (λ ($x = 0.28\ \mu$m) = 320 nm, λ ($x = 0.4\ \mu$m) = 360 nm, λ ($x = 0.9\ \mu$m) = 370 nm, λ ($x = 1.8\ \mu$m) = 380 nm). (d) Plot of IPCE *versus* $1-10^{-\alpha x}$ (absorption efficiency, η_{e^-/h^+}) shows that the IPCE has a linear correlation near the band edge (λ = 410 nm) of the TiO_2. IPCE (%) = 82.58 $\times$ ($1 - 10^{-\alpha x}$) $-$ 0.485, R^2 = 0.993.

oxidation reaction and the flat band potential,[24,26] which were not influenced by the length of the nanowires or the growth time. Nanowires showed an increase in photocurrent with length, which is expected since longer nanowires have a longer optical pathway. The highest photocurrent (0.73 mA/cm^2 at 1.5 V *vs* RHE) was observed for 1.8 μm long nanowires within the experimental conditions. This is 40% of the maximum photocurrent density (1.8 mA/cm^2) for rutile TiO_2 under AM1.5G simulated sunlight illumination, assuming a quantum efficiency (QE) of 100% above the band gap (3.0 eV).

The photocurrent densities (1.5 V *vs* RHE) are plotted *versus* nanowire length in Figure 2b, showing that the photocurrent does not increase linearly with length. For example, the photocurrent increased by 0.275 mA/cm^2 (from 0.125 to 0.4 mA/cm^2) when the length grew from 0.28 to 0.4 μm, while it increased only by 0.12 mA/cm^2 (from 0.61 to 0.73 mA/cm^2) when the length grew from 0.9 to 1.8 μm. The shape of the curve implies that the photocurrent is close to saturation with a length of 1.8 μm for TiO_2 nanowires.

The effect of nanowire length on photocurrent can be discussed in more detail by comparing the absorption and IPCE dependence of TiO_2 nanowires on the incident light wavelength (λ) (Figure 2c,d). The absorption of light depends on the optical absorption length (x) and the absorption coefficient (α) where Im(n_s) is imaginary part of the refractive index (eqs 2 and 3).

$$A = \alpha x = -\log\left(\frac{I}{I_0}\right) \quad (2)$$

$$\alpha = \frac{4\pi \mathrm{Im}(n_s)}{\lambda} \quad (3)$$

The IPCE or external quantum efficiency (EQE) takes into account three efficiencies: photon absorptance (η_{e^-/h^+}), charge transport within semiconductor materials ($\eta_{transport}$), and charge transfer at the semiconductor/electrolyte interface ($\eta_{transfer}$) (eq 4).[27] Here, the

efficiency of photon absorptance is defined as the fraction of electron−hole pair generation per incident photon flux, which can be related to the absorption length (eq 5).

$$\begin{aligned} \mathrm{IPCE}(\lambda) &= \mathrm{EQE}(\lambda) \\ &= \eta_{e^-/h^+}(\lambda) \times \eta_{transport}(\lambda) \times \eta_{transfer}(\lambda) \end{aligned} \quad (4)$$

$$\eta_{e^-/h^+} = \frac{I_0 - I}{I_0} = 1 - \frac{I}{I_0} = 1 - 10^{-\alpha x} \quad (5)$$

The IPCE was measured at 1.5 V *vs* RHE where the photocurrents of the nanowires were saturated (Figure 2c). As the nanowires increase in length, the enhancement in IPCE is significant. This is especially true between λ = 380−420 nm since $\alpha(\lambda)$ of rutile TiO_2 decreases significantly in this region.[28] At λ = 380 nm, the IPCE increases from 4.2 to 57.0% as the length of the nanowires increases. A plot of IPCE *versus* efficiency of photon absorptance ($\eta_{e^-/h^+} = 1-10^{-\alpha x}$) at λ = 410 nm is illustrated in Figure 2d, where α(410 nm) = 0.5×10^3/cm,[29] assuming TiO_2 nanowires have the same absorption length as bulk TiO_2, and x is the average length of the nanowires. A strong linear correlation (R^2 = 0.993) between IPCE and $1-10^{-\alpha x}$ is observed except for the IPCE of 0.28 μm long nanowire arrays. The IPCE for the 0.28 μm sample is lower than the expected value because the nanowires do not cover the FTO substrate entirely (Figure 1a). The strong linear correlation verifies that the EQE of TiO_2 nanowire arrays is strongly influenced by the absorption of photons near the band gap.

The maximum IPCE for TiO_2 nanowires shifts in wavelength as the length of nanowires increases, indicating some changes in dynamics for carrier collection (Figure 2c). Nanowires which are 1.8 μm long have a maximum IPCE at 380 nm which is consistent with other reports for rutile TiO_2.[19] Due to efficient light absorption with a larger α,[28,29] an increase in IPCE is expected at shorter wavelengths. However, at the shorter wavelengths, the IPCE of TiO_2 decreases since a fraction of the photogenerated majority carriers in the depletion region can diffuse to the electrolyte interface against the electric field and thus oppose the photocurrent by recombining with holes.[30] The effects of electron diffusion losses are significant when the majority carrier's mobility is low and/or there is a high density of interface states which creates a large recombination velocity. Higher energy photons at wavelengths shorter than 380 nm are mainly absorbed by the top part of the nanowires. Therefore, a lower charge collection efficiency is expected because these electrons must travel the entire length of the nanowire to reach the FTO back contact. As the length of TiO_2 nanowires decreases, the maximum IPCE shifts to shorter wavelengths. This implies that $\eta_{transport}(\lambda)$ and $\eta_{transfer}(\lambda)$ are more important factors for the IPCE in the short wavelength region while $\eta_{e^-/h^+}(\lambda)$ is more significant for incident wavelengths near the band gap. Therefore, the longer nanowire arrays can enhance the EQE by increasing the absorption efficiency ($1-10^{-\alpha x}$) but are unfavorable for charge collection at the short wavelengths. This also explains the trend of photocurrent dependence on nanowire length that we observed in Figure 2b. For TiO_2 nanowire arrays, it is necessary to improve the charge collection efficiency before growing longer nanowire arrays to increase the energy conversion efficiency.

ALD was used to deposit a TiO_2 shell on rutile TiO_2 nanowires to increase charge collection efficiency by reducing surface states.[10,22] A series of shell thicknesses were deposited at 300 °C on 1.8 μm long TiO_2 nanowires to examine the dependence of photocatalytic performance on the shell thickness. Figure 3a shows a high-resolution transmission electron microscopy (HRTEM) image and the corresponding selected area electron diffraction (SAED) pattern of a bare TiO_2 nanowire, confirming that nanowires are grown in the ⟨001⟩ direction with the rutile crystal structure. When 60 cycles of TiO_2 is deposited, the ALD shell is about 5−7 nm thick and is composed of crystalline particles and an amorphous layer (Figure 3b). With 150 cycles of TiO_2, no amorphous layer was observed and epitaxial grains of rutile TiO_2 extend 13−15 nm from the surface of the TiO_2 nanowire (Figure 3c and Figure S1 in the Supporting Information). When 300 cycles of TiO_2 is deposited, the shell has a polycrystalline anatase structure (d_{101} = 3.5 ± 0.1 Å) with a shell thickness of 25−30 nm (Figure 3d,e). From the TEM study, we find that a phase transition of rutile to anatase TiO_2 happens as thicker ALD layers are deposited, although rutile is more thermodynamically stable. Different phases of ALD TiO_2 have been reported depending on the substrate and the growth temperature.[31] More structural studies are required to understand the unusual phase transitions of ALD TiO_2 on rutile nanowire surfaces.

X-ray diffraction patterns of the ALD TiO_2 samples are consistent with TEM characterization showing anatase formation as the shell thickness increases. As-grown TiO_2 nanowires and TiO_2 nanowires with 150 ALD cycles have the rutile 101 and FTO substrate peaks (Figure 3). However, the anatase 101 peak was observed for the sample with 300 ALD cycles, indicating that the shell has the anatase phase with primarily the 101 orientation. Similarly, Raman spectroscopy (Figure S2) of TiO_2 nanowires with 300 ALD cycles shows characteristic peaks associated with the anatase phase (141 cm^{-1} E_g and 515 cm^{-1} A_{1g} and B_{1g}),[32] while only rutile peaks were observed with 150 ALD cycles.

To examine the dependence of the PEC water oxidation properties of ALD-coated TiO_2 nanowires on shell thickness, we compared the photocurrents of 1.8 μm nanowires with different shell thicknesses

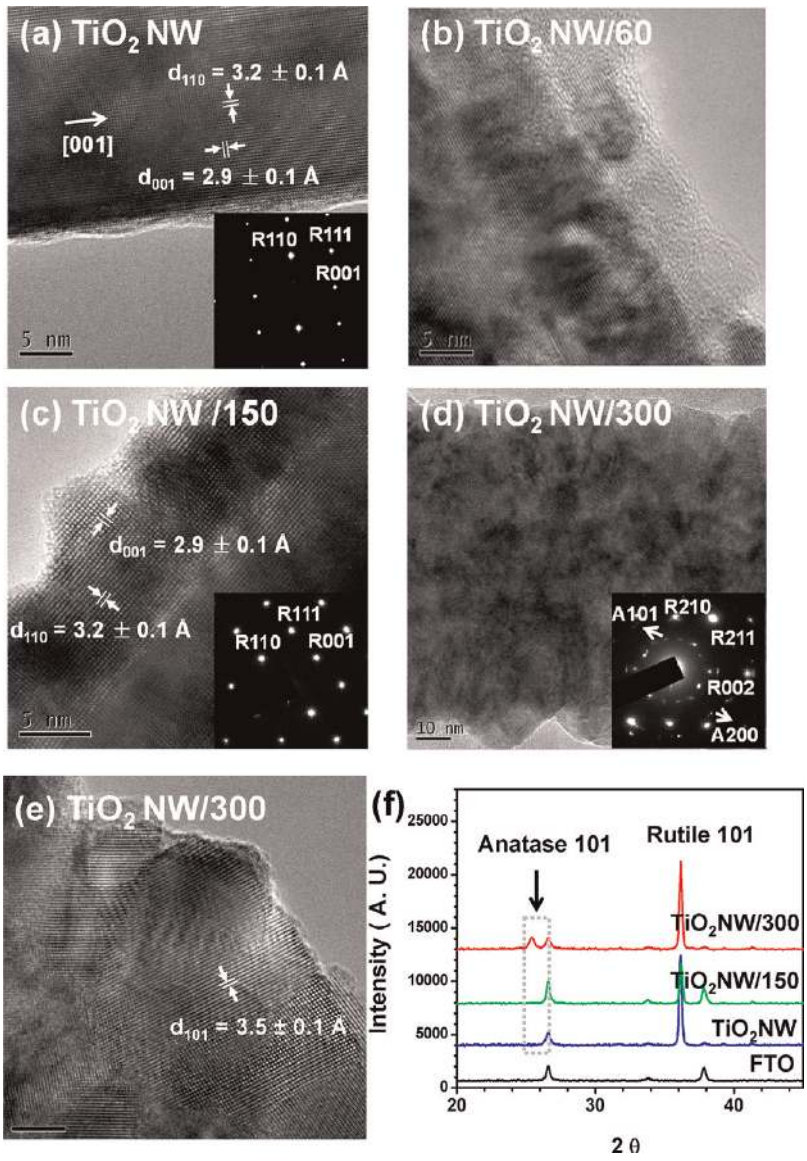

Figure 3. HRTEM images of TiO_2 nanowires with (a) no shell and nanowires with (b) 60, (c) 150, (d,e) and 300 ALD cycles of TiO_2. HRTEM images as well as SAED patterns (insets) show a phase change for the shell from rutile (150 cycles) to anatase (300 cycles) as the thickness increases. (f) X-ray diffraction patterns confirm the appearance of the anatase (101) peak.

(Figure 4a). With a thin shell (60−100 cycles), the photocurrent (1.5 V *vs* RHE) is decreased up to 70% most likely because the amorphous layers formed at these thicknesses can block charge transfer across the TiO_2/electrolyte junction. Also, the continuous amorphous shell can decrease the photovoltage at the TiO_2/electrolyte junction which is the driving force for charge separation. As the shell increases in thickness and crystallizes into pure rutile TiO_2 (150 cycles), the current density reaches a maximum of 1.1 mA/cm^2 (1.5 V *vs* RHE). With this current density increase, ALD-coated TiO_2 nanowires can obtain 61% of the maximum photocurrent (1.8 mA/cm^2) under AM1.5G simulated sunlight illumination. We propose that the performance increase is due to the role of the epitaxial rutile shell in suppressing surface recombination rates by passivating charge trapping sites.

After the shell undergoes a phase transition to anatase (300−450 cycles), the photooxidation activity clearly decreases with increasing thickness. This implies that the anatase shell blocks efficient hole transfer from the rutile core to the electrolyte. To understand why the anatase shell is decreasing the overall photocatalytic activity, we can consider both the structural and electronic characteristics of the junction between the shell and the core. First, we can examine the structure of the core@shell nanowires from HRTEM images. Figure 3d shows that the anatase shell does not grow epitaxially from the rutile core due to lattice mismatch. The polycrystalline nature of the anatase shell can introduce new interfacial states and grain boundaries which can decrease the efficiency of hole transfer at the interface. Second, we can consider the band alignment between the two phases of TiO_2 to

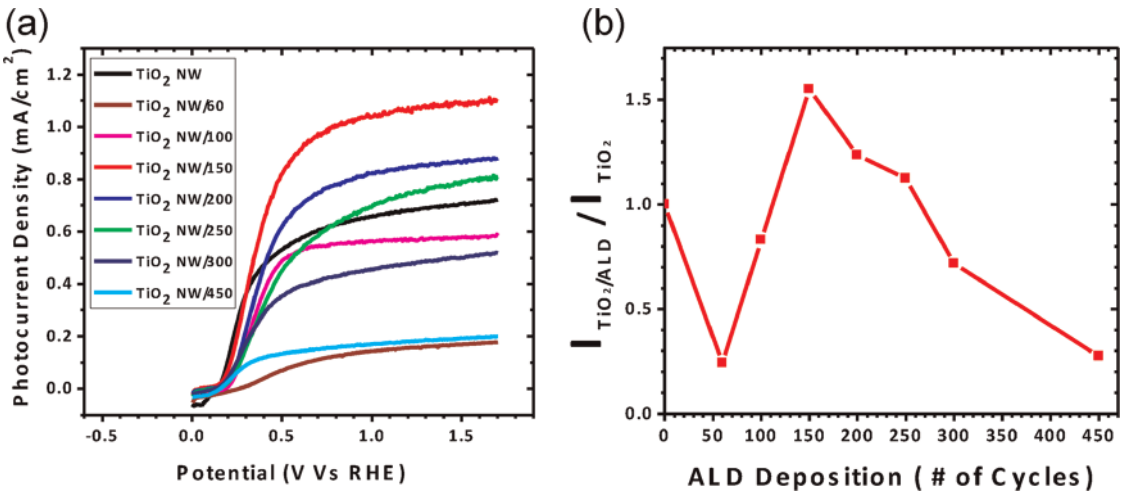

Figure 4. (a) Plots of photocurrent densities *vs* RHE for 1.8 μm long TiO_2 nanowire arrays electrodes with various ALD cycles (60, 100, 150, 200, 250, 300, and 450 cycles). (b) Plot of normalized photocurrent densities ($I_{TiO_2/ALD}/I_{TiO_2}$) *vs* the number of ALD cycles shows a maximum enhancement at 150 cycles. Normalized current densities were obtained at 1.5 V *vs* RHE.

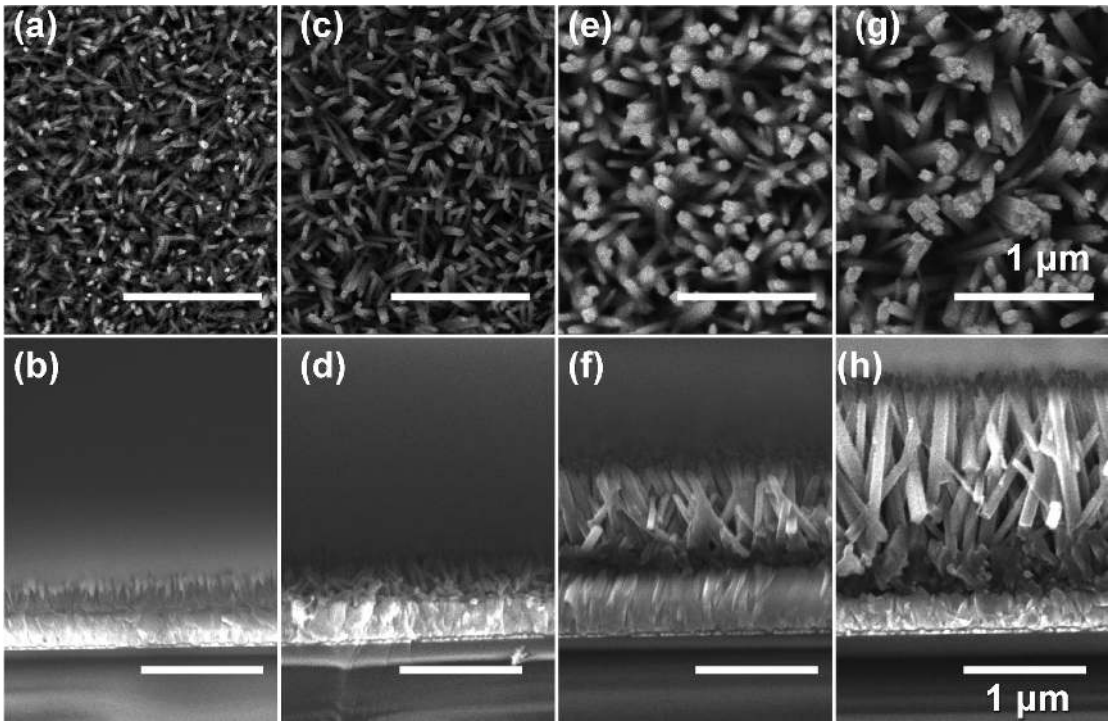

Figure 5. Top-down and cross sectional SEM images of TiO_2 nanowire arrays, with 150 ALD cycles, grown on FTO substrates. The core TiO_2 nanowire arrays were grown for 50 (a,b), 60 (c,d), 80 (e,f), and 150 min (g,h) at 200 °C. Average nanowire lengths were 0.28, 0.4, 0.9, and 1.8 μm, respectively.

determine whether charge transfer is favorable. Anatase TiO_2 (3.2 eV) has a 0.2 eV larger band gap when compared to rutile TiO_2 (3.0 eV). Since both anatase and rutile phases are typical n-type semiconductors, their Fermi levels can be considered to be close to their conduction band edges in energy.[33,34] Therefore, after contact and thermal equilibrium where the Fermi levels of rutile and anatase are equal, the valence band of rutile should be higher in energy than that of anatase. Because of this offset, the hole feels an energetic barrier to transfer from rutile to anatase, and we expect the photocatalytic activity to decrease when the anatase shell completely covers the rutile core. This is in contrast to mixtures of rutile and anatase phases, which have higher activity than either pure phase, because both phases in that geometry are exposed to the electrolyte.[15,35] These results emphasize that the phase of the ALD shell can have a significant influence on photocatalytic activity. On the basis of these results, we conclude that an epitaxial rutile ALD shell can

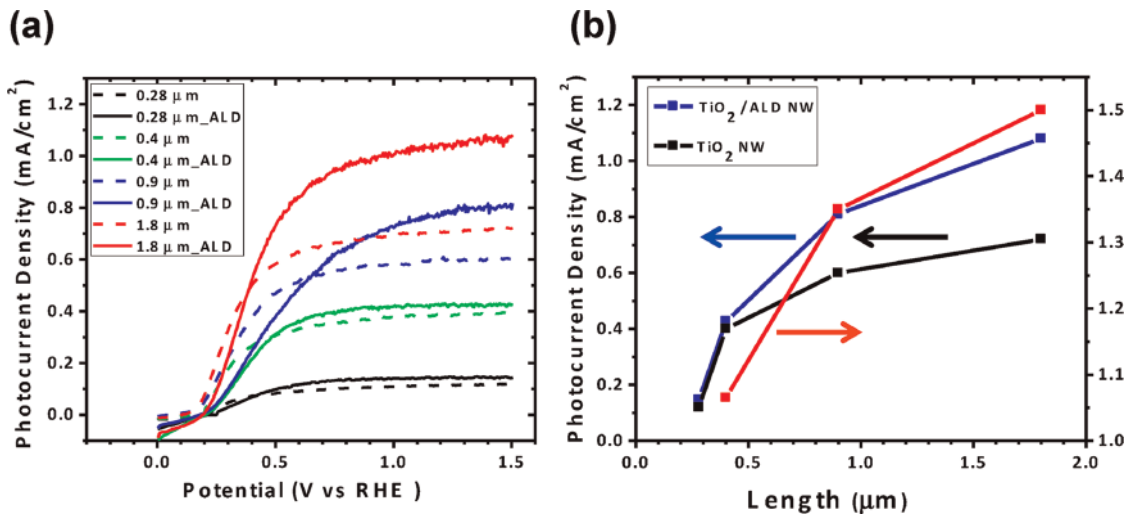

Figure 6. (a) Photocurrent densities for TiO_2 nanowires of different lengths are shown for nanowires with and without 150 ALD cycles. (b) Plots of photocurrent densities (1.5 V *vs* RHE) and enhancement factors ($I_{TiO_2/ALD}/I_{TiO_2}$) *vs* the length of TiO_2 nanowire arrays.

increase the water splitting efficiency of rutile TiO_2 nanowires.

The normalized photocurrent densities ($I_{TiO_2/ALD}/I_{TiO_2}$) at 1.5 V *vs* RHE were also compared *versus* the number of ALD cycles (Figure 4b) to show the change in performance between as-made and ALD-coated nanowires. The photocurrents were enhanced compared to bare TiO_2 nanowire arrays between 150−250 cycles of ALD coating, while the photocurrent decreased for all other thicknesses. A maximum of 1.5 times enhancement was obtained with 150 ALD cycles.

Additional PEC measurements were performed on TiO_2 nanowires with different lengths but the same shell thickness (150 cycles) to examine the effects of the epitaxial rutile ALD shell on photocatalytic activity. Top-down and cross sectional SEM images were taken of 0.28, 0.4, 0.9, and 1.8 μm long TiO_2 nanowires with 150 ALD cycles (Figure 5). The cross section images show that the nanowire arrays are dense and slightly off-vertical. Figure 6a shows the photocurrent densities of TiO_2 nanowire arrays with (solid lines) and without (dot lines) ALD coating. The photocurrent is enhanced with ALD coating regardless of nanowire length, although the amount of increase is different. The enhancement factors, defined as the normalized photocurrent densities ($I_{TiO_2/ALD}/I_{TiO_2}$) at 1.5 V *vs* RHE, were plotted *versus* the length of the nanowire arrays (Figure 6b) to quantify the increase in performance. The enhancement factor increases with nanowire length between 0.4 and 1.8 μm. It is most likely higher for the 0.28 μm long nanowires because the amount of TiO_2 deposited is relatively large since the FTO surface is not completely covered by nanowires.

To determine the effect of the ALD shell on the EQE of different nanowire lengths, we measured the IPCE of TiO_2 nanowires with and without ALD coating (Figure 7a). Nanowires with the ALD shell show varying levels of increase in IPCE depending on the nanowire length as well as the wavelength of light. The most prominent enhancement in IPCE was observed at shorter wavelengths (below the peak IPCE wavelength) with longer nanowires. For example, the IPCE of 1.8 μm long TiO_2 nanowire arrays with ALD coating is enhanced significantly at $\lambda < 380$ nm, although it remains similar at higher wavelengths near the band gap of rutile TiO_2. By comparing the wavelength dependence of the enhancement in IPCE from ALD coating (Figure 7a) to optical measurements (Figure 7b), we can determine whether they are correlated. Figure 7b shows the optical properties of TiO_2 nanowire arrays on the FTO substrate with and without ALD coating. Due to a thick FTO/glass substrate, the scattering was not completely accounted for in the transmittance or reflectance spectra, so 100 − reflectance − transmission (%) indicates the absorption plus scattering. The absorption plus scattering for 1.8 μm long TiO_2 nanowire arrays is higher than 98% at $\lambda < 370$ nm even without the ALD shell, so the improvement in absorption from ALD is minimal in this region. However, the ALD shell enhances the IPCE of TiO_2 nanowires at $\lambda < 390$ nm despite a minute amount of increase in the absorption of light. At longer wavelengths ($\lambda >$ 380 nm), TiO_2 nanowires with 150 ALD cycles have slightly higher absorption plus scattering. In contrast, the IPCE is similar with or without the ALD shell near the band edge region ($\lambda > 390$ nm). Therefore, we can conclude that the increase in IPCE is not due to a change in absorption efficiency (η_{e^-/h^+}).

Instead, the enhancement at $\lambda < 390$ nm from the ALD coating could be due to several factors affecting the charge collection efficiency including $\eta_{transport}(\lambda)$ and $\eta_{transfer}(\lambda)$. First, the interface recombination velocity is expected to decrease when the ALD shell passivates surface states on TiO_2 nanowires. Salvador

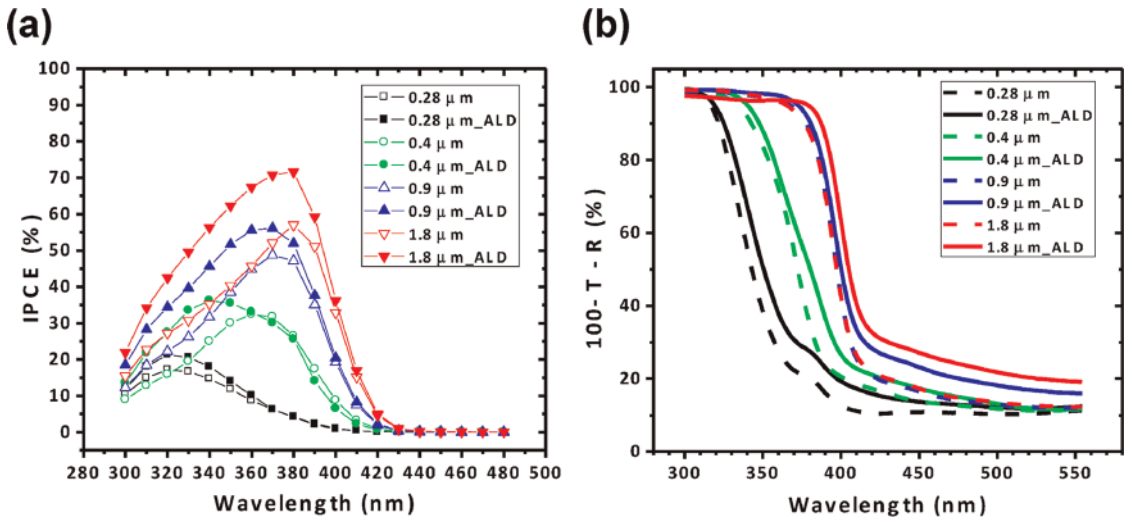

Figure 7. (a) IPCE (1.5 V *vs* RHE) for TiO_2 nanowires of different lengths is shown for nanowires with and without 150 ALD cycles. The EQE is mainly enhanced at λ = 320−380 nm. (b) 100 − transmission − reflection (%) for the corresponding TiO_2 nanowire arrays.

reported that the electron−hole recombination in TiO_2 is governed by a trapping mechanism in which the hole lifetime (τ_p) depends on the density of recombination centers.[10] The minority carrier diffusion length (L_p) is related to the lifetime by the following equation: $L_p = (D_p\tau_p)^{1/2}$, where D_p is the diffusivity.[20] Passivation can increase the diffusion length of the hole by reducing recombination and can therefore increase the size of the active region since the active region is $L_p + W$ (width of the space-charge region), by decreasing electron diffusion losses.[30]

Also, an increase in semiconductor/electrolyte junction area has been demonstrated to be beneficial[14,19] for water splitting since the increase in surface area allows for holes to transfer more efficiently to the electrolyte. The HRTEM image in Figure 3c clearly shows that the ALD shell increases the surface area when compared to the as-made TiO_2 nanowire (Figure 3a) and provides a larger area for the water oxidation reaction to happen. The rough surface also indicates that the sidewall of ALD-coated (150 cycles) TiO_2 nanowires has other facets exposed in addition to the (110) surface, which is the exposed side facet of the bare TiO_2 nanowires. Reports show some photocatalytic activity dependence on the crystal facet of rutile TiO_2[36,37] due to a disparity in hole reactivity on different surfaces. Therefore, it is possible that the activity of core/shell nanowires can be affected by the mixture of different crystal facets. These synergistic effects show that ALD coating could contribute to an increase in charge collection efficiency.

Finally, we previously discussed that the IPCE of longer TiO_2 nanowires decreases at shorter wavelengths due to charge collection losses (Figure 2c). The photocurrent results show that the longer nanowire arrays are affected the most by charge collection losses but have the highest enhancement factors (Figure 6b) from ALD coating. These results along with the increase in IPCE suggest that ALD coating can increase the charge collection efficiency for nanowires. The enhancement factor is decreased for shorter nanowire arrays because the increase in IPCE is observed at shorter wavelengths, which represent only a small fraction of sunlight.

CONCLUSION

In conclusion, we demonstrated that the water splitting activity of TiO_2 nanowire arrays depends on their length and surface properties. Photocurrent measurements showed a nonlinear increase in photocurrent with nanowire length and approached saturation with a length of 1.8 μm. The IPCE of TiO_2 nanowires increased linearly *versus* $1-10^{-\alpha\times\text{length}}$ with near band gap illumination (λ = 410 nm) due to an increase in the absorption of light (η_{e^-/h^+}). However, the IPCE decreases significantly at shorter wavelengths for longer nanowires because of poor charge collection efficiency. To improve charge collection efficiency, a TiO_2 ALD layer was deposited on the TiO_2 nanowire arrays. The ALD shell showed different phases from amorphous to epitaxial rutile to polycrystalline anatase TiO_2 depending on the thickness of the shell. Amorphous and anatase TiO_2 shells decreased the photocurrent when compared to as-made nanowires. However, epitaxial grains of rutile shells showed a photocurrent enhancement of 1.5 times, demonstrating the importance of the interface between the core and shell. By comparing optical and IPCE measurements, we determined that the ALD shell does not significantly influence the absorption of light. We suggest that the large enhancement is due to improved charge collection efficiency from passivation of defect sites and an increase in surface area. These results show

that the geometric and surface properties of semiconductors must be considered to achieve high water splitting efficiency since these properties can affect all of the processes that affect the EQE (photon absorptance, charge transport, and charge separation) during PEC reactions.

METHODS

Hydrothermal TiO_2 Nanowire Array Growth. TiO_2 nanowire photoanodes were prepared by growing nanowire arrays on FTO.[25] Deionized water (5 mL) was mixed with hydrochloric acid (5 mL, 36.5−38 wt %) and stirred for 5 min before titanium isopropoxide (0.167 mL, TTIP, 97% Aldrich) was added. After stirring for 6 h, the mixture solution was transferred to a Teflon-lined stainless steel autoclave. Clean FTO/glass substrates (area 5 cm^2) were immersed with the conducting side face down. The autoclave was put in an oven at a temperature of 200 °C and was taken out from the oven after 50−150 min to control the nanowire length. After the autoclave was cooled for 2 h to room temperature, the FTO substrate was rinsed with DI water and subsequently annealed at 400 °C for 1 h in air. TiO_2 nanowires grew only on the side of the FTO substrate where it was immersed in the growth solution. The final area of the nanowire arrays was approximately 2.6−2.8 cm^2.

ALD TiO_2 Shell Deposition. The TiO_2 samples were cleaned with isopropyl alcohol and DI water followed by drying with N_2 gas using a gun before ALD deposition. The exposed bare FTO substrate, where no TiO_2 nanowires were grown, was protected with aluminum foil and kapton tape to avoid direct deposition on the FTO surface. Shells were deposited on TiO_2 nanowire arrays by using a homemade ALD system at 300 °C with $TiCl_4$ (99.990%, Alfa) and pure DI water as the precursors. To control the thickness, the number of ALD cycles was varied from 60 to 450 cycles. The ALD shell was characterized with X-ray diffraction (Bruker AXS D8 Advance), Raman spectroscopy (HORIBA Jobin Yvon Inc.), and high-resolution transmission electron microscopy (JEOL JEM-2100 LaB6).

Photoelectrochemical Measurement. Photocurrents of TiO_2 nanowire electrodes were measured with a potentiostat (Gamry ref 600) using a Ag/AgCl reference electrode and a Pt mesh counter electrode. A 300 W Xe lamp (Newport, 6258) was coupled with an AM 1.5 filter (Newport, 81094) to simulate sunlight, and a diffuser was used for uniform illumination intensity (100 mW/cm^2) over the entire TiO_2 nanowire electrode area (2.6−2.8 cm^2). TiO_2 nanowire photoanodes were immersed in 1 M NaOH and illuminated through a quartz window of a glass cell. For the incident photon to current conversion efficiency (IPCE) measurement, a 300 W Xe lamp was coupled with a monochromator (Newport, cornerstone 130), and the incident light intensity was measured with a calibrated Si photodiode. Here, the IPCE was calculated from the photocurrents measured at 1.5 V *vs* RHE according to the following equation.

$$\mathrm{IPCE} = \frac{I_{ph}\ (\mathrm{mA/cm^2}) \times 1239.8\ (\mathrm{V} \times \mathrm{nm})}{P_{mono}\ (\mathrm{mW/cm^2}) \times \lambda\ (\mathrm{nm})}$$

Optical Measurement. The absorption properties of TiO_2 nanowire arrays on FTO substrates were obtained with an integrating sphere (ISR-3100, Shimadzu Corp.) and UV−vis spectrophotometer (UV-3101 PC, Shimadzu Corp.). Since the FTO substrate was 3 mm thick, scattering was not completely accounted for in the transmission or reflection spectra. Therefore, absorption plus residual scattering was calculated from 100 − reflectance − transmission (%).

Conflict of Interest: The authors declare no competing financial interest.

Acknowledgment. This work was supported by the Director, Office of Science, Office of Basic Energy Sciences, Materials Sciences and Engineering Division, of the U.S. Department of Energy under Contract No. DE-AC02-05CH11231.

Supporting Information Available: High-resolution transmission electron microscope image of a TiO_2 NW with 150 ALD cycles, and Raman shifts of TiO_2 nanowires with 150 and 300 ALD cycles. This material is available free of charge *via* the Internet at http://pubs.acs.org.

REFERENCES AND NOTES

1. Walter, M. G.; Warren, E. L.; Mckone, J. R.; Boettcher, S. W.; Santori, E. A.; Lewis, N. S. Solar Water Splitting Cells. *Chem. Rev.* **2010**, *110*, 6446–6473.
2. Fukishima, A.; Honda, K. Electrochemical Photolysis of Water at a Semiconductor Electrode. *Nature* **1972**, *238*, 37–38.
3. Nozik, A. J. Photoelectrolysis of Water Using Semiconducting TiO_2 Crystals. *Nature* **1975**, *257*, 384–386.
4. Nowotny, J.; Sorrell, C. C.; Sheppard, L. R.; Bak, T. Solar-Hydrogen: Environmentally Safe Fuel for the Future. *Int. J. Hydrogen Energy* **2005**, *30*, 521–544.
5. Ni, M.; Leung, M. K.; Leung, D. Y.; Sumathy, K. A Review and Recent Developments in Photocatalytic Water-Splitting Using TiO_2 for Hydrogen Production. *Renewable Sustainable Energy Rev.* **2007**, *11*, 401–425.
6. Wang, G.; Wang, H.; Ling, Y.; Tang, Y.; Yang, X.; Fitzmorris, R. C.; Wang, C.; Zhang, J. Z.; Li, Y. Hydrogen-Treated TiO_2 Nanowire Arrays for Photoelectrochemical Water Splitting. *Nano Lett.* **2011**, *11*, 3026–3033.
7. Hoang, S.; Guo, S.; Hahn, N. T.; Bard, A. J.; Mullins, C. B. Visible Light Driven Photoelectrochemical Water Oxidation on Nitrogen-Modified TiO_2 Nanowires. *Nano Lett.* **2012**, *12*, 26–32.
8. Linsebigler, A. L.; Lu, G.; Yates, J. T. Photocatalysis on TiO_2 Surfaces: Principles, Mechanisms, and Selected Results. *Chem. Rev.* **1995**, *95*, 735–758.
9. Hendry, E.; Koeberg, M.; O'Regan, B.; Bonn, M. Local Field Effects on Electron Transport in Nanostructured TiO_2 Revealed by Terahertz Spectroscopy. *Nano Lett.* **2006**, *6*, 755–759.
10. Salvador, P. Hole Diffusion Length in n-TiO_2 Single Crystals and Sintered Electrodes: Photoelectrochemical Determination and Comparative Analysis. *J. Appl. Phys.* **1984**, *55*, 2977–2985.
11. Zhu, J.; Zäch, M. Nanostructured Materials for Photocatalytic Hydrogen Production. *Curr. Opin. Colloid Interface Sci.* **2009**, *14*, 260–269.
12. Liu, G.; Sun, C.; Yang, H. G.; Smith, S. C.; Wang, L.; Lu, G. Q.; Cheng, H. M. Nanosized Anatase TiO_2 Single Crystals for Enhanced Photocatalytic Activity. *Chem. Commun.* **2010**, *46*, 755–757.
13. Yu, J.; Zhang, L.; Cheng, B.; Su, Y. Hydrothermal Preparation and Photocatalytic Activity of Hierarchically Sponge-like Macro-/Mesoporous Titania. *J. Phys. Chem. C* **2007**, *111*, 10582–10589.
14. Shi, J.; Hara, Y.; Sun, C.; Anderson, M. A.; Wang, X. Three-Dimensional High-Density Hierarchical Nanowire Architecture for High-Performance Photoelectrochemical Electrodes. *Nano Lett.* **2011**, *11*, 3413–3419.
15. Liu, M.; Snapp, N.; Park, H. Water Photolysis with a Cross-Linked Titanium Dioxide Nanowire Anode. *Chem. Sci.* **2011**, *2*, 80–87.
16. Khan, S. U.; Sultana, T. Photoresponse of n-TiO_2 Thin Film and Nanowire Electrodes. *Sol. Energy Mater. Sol. Cells* **2003**, *76*, 211–221.
17. Feng, X.; Shankar, K.; Varghese, O. K.; Paulose, M.; Latempa, T. J.; Grimes, C. A. Vertically Aligned Single Crystal TiO_2 Nanowire Arrays Grown Directly on Transparent Conducting Oxide Coated Glass: Synthesis Details and Applications. *Nano Lett.* **2008**, *8*, 3781–3786.

18. Shankar, K.; Basham, J. I.; Allam, N. K.; Varghese, O. K.; Mor, G. K.; Feng, X.; Paulose, M.; Seabold, J. A.; Choi, K. S.; Grimes, C. A. Recent Advances in the Use of TiO_2 Nanotube and Nanowire Arrays for Oxidative Photoelectrochemistry. *J. Phys. Chem. C* **2009**, *113*, 6327–6359.
19. Cho, I. S.; Chen, Z.; Forman, A. J.; Kim, D. R.; Rao, P. M.; Jaramillo, T. F.; Zheng, X. Branched TiO_2 Nanorods for Photoelectrochemical Hydrogen Production. *Nano Lett.* **2011**, *11*, 4978–4984.
20. Law, M.; Greene, L. E.; Radenovic, A.; Kuykendall, T.; Liphardt, J.; Yang, P. ZnO−Al_2O_3 and ZnO−TiO_2 Core−Shell Nanowire Dye-Sensitized Solar Cells. *J. Phys. Chem. B* **2006**, *110*, 22652–22663.
21. Schmidt, J.; Merkle, A.; Hoex, B.; van de Sanden, M. C. M.; Kessels, W. M. M.; Brendel, R. Atomic-Layer-Deposited Aluminum Oxide for the Surface Passivation of High-Efficiency Silicon Solar Cells. *Conf. Rec. IEEE Photovoltaic Spec. Conf.* **2008**, 10.1109/PVSC.2008.4922636.
22. Formal, F. L.; Tétreault, N.; Cornuz, M.; Moehl, T.; Grätzel, M.; Sivula, K. Passivating Surface States on Water Splitting Hematite Photoanodes with Alumina Overlayers. *Chem. Sci.* **2011**, *2*, 737–743.
23. Paracchino, A.; Laporte, V.; Sivula, K.; Grätzel, M.; Thimsen, E. Highly Active Oxide Photocathode for Photoelectrochemical Water Reduction. *Nat. Mater.* **2011**, *10*, 456–461.
24. Hwang, Y. J.; Boukai, A.; Yang, P. High Density n-Si/n-TiO_2 Core/Shell Nanowire Arrays with Enhanced Photoactivity. *Nano Lett.* **2009**, *9*, 410–415.
25. Liu, B.; Aydil, E. S. Growth of Oriented Single-Crystalline Rutile TiO_2 Nanorods on Transparent Conducting Substrates for Dye-Sensitized Solar Cells. *J. Am. Chem. Soc.* **2009**, *131*, 3985–3990.
26. Dutoit, E. C.; Cardon, F.; Gomes, W. P. Electrochemical Properties of the Semiconducting TiO_2 (Rutile) Single Crystal Electrode. *Ber. Bunsen-Ges. Phys. Chem.* **1976**, *80*, 475–481.
27. Chen, Z. B.; Jaramillo, T. F.; Deutsch, T. G.; Kleiman-Shwarsctein, A.; Forman, A. J.; Gaillard, N.; Garland, R.; Takanabe, K.; Heske, C.; Sunkara, M.; *et al.* Accelerating Materials Development for Photoelectrochemical Hydrogen Production: Standards for Methods, Definitions, and Reporting Protocols. *J. Mater. Res.* **2010**, *25*, 3–16.
28. Persson, C.; Silva, A. F. Strong Polaronic Effects on Rutile TiO_2 Electronic Band Edges. *Appl. Phys. Lett.* **2005**, *86*, 231912.
29. Thomazi, F.; Roman, L. S.; Silva, A. F.; Persson, C. Optical Absorption of Rutile SnO_2 and TiO_2. *Phys. Status Solidi C* **2009**, *6*, 2740–2742.
30. Reichman, J. Collection Efficiency of Low-Mobility Solar Cells. *Appl. Phys. Lett.* **1981**, *38*, 251–253.
31. Cheng, H. E.; Hsu, C. M.; Chen, Y. C. Substrate Materials and Deposition Temperature Dependent Growth Characteristics and Photocatalytic Properties of ALD TiO_2 Films. *J. Electrochem. Soc.* **2009**, *156*, D275–D278.
32. Ma, H. L.; Yang, J. Y.; Dai, Y.; Zhang, Y. B.; Lu, B.; Ma, G. H. Raman Study of Phase Transformation of TiO_2 Rutile Single Crystal Irradiated by Infrared Femtosecond Laser. *Appl. Surf. Sci.* **2007**, *253*, 7497–7500.
33. Gerischer, H. Solar Photoelectrolysis with Semiconductor Electrodes. *Solar Energy Conversion*; Springer: Berlin, 1979; pp115−172.
34. Radecka, M.; Rekas, M.; Trenczek-Zajac, A.; Zakrzewska, K. Importance of the Band Gap Energy and Flat Band Potential for Application of Modified TiO_2 Photoanodes in Water Photolysis. *J. Power Sources* **2008**, *181*, 46–55.
35. van der Meulen, T.; Mattson, A.; Österlund, L. A Comparative Study of the Photocatalytic Oxidation of Propane on Anatase, Rutile, and Mixed-Phase Anatase−Rutile TiO_2 Nanoparticles: Role of Surface Intermediates. *J. Catal.* **2007**, *251*, 131–144.
36. Nakamura, R.; Ohashi, N.; Imanishi, A.; Osawa, T.; Matsumoto, Y.; Koinuma, H.; Nakato, Y. Crystal-Face Dependences of Surface Band Edges and Hole Reactivity, Revealed by Preparation of Essentially Atomically Smooth and Stable (110) and (100) n-TiO_2 (Rutile) Surfaces. *J. Phys. Chem. B* **2005**, *109*, 1648–1651.
37. Wilson, J. N.; Idriss, H. Structure Sensitivity and Photocatalytic Reactions of Semiconductors. Effect of the Last Layer Atomic Arrangement. *J. Am. Chem. Soc.* **2002**, *124*, 11284–11285.